CrystEngComm

Dynamic Article Links

Cite this: *CrystEngComm*, 2011, **13**, 4282

www.rsc.org/crystengcomm

PAPER

Catalyst/dopant-free growth of ZnO nanobelts with different optical properties from nanowires grown *via* a catalyst-assisted method

B. Q. Cao,*[a] Z. M. Liu,[a] H. Y. Xu,[a] H. B. Gong,[a] D. Nakamura,[b] K. Sakai,[c] M. Higashihata[b] and T. Okada*[b]

Received 14th January 2011, Accepted 22nd February 2011
DOI: 10.1039/c1ce05058c

The paper reported a simple but effective gold catalyst-tailored chemical vapour deposition (CVD) method to grow ZnO nanowires and nanobelts with different photoluminescence (PL) behaviours. ZnO nanowires along the *c*-axis were synthesized *via* a gold catalyst-assisted CVD method through the conventional vapour–liquid–solid (VLS) mechanism. But, ZnO nanobelts grew along the *a*-axis enclosed with $\{01\bar{1}0\}$ and {0001} base planes without using any catalyst or dopant through the vapour–solid (VS) mechanism. The nanowires and nanobelts were proved to be of different optical quality, which was related with their growth process. Besides the different origin of the near-band-gap emission at room temperature, laser emission was only observed from ZnO nanobelts while the nanowires show anomalous photoluminescence behaviour under higher excitation density.

1. Introduction

Due to the possibility of multiple and switchable growth directions of the hexagonal wurtzite structure and the high ionicity of its polar surfaces, ZnO exhibits a wide range of novel structures that can be grown by tuning the growth conditions.[1–11] Among them, nanobelts and nanowires are the most important candidates for potential optoelectronic applications. The controlled growth of different ZnO nanostructures as nanodevice building blocks and their optical properties are two important issues in this area.[12,13] Catalyst-assisted vapour phase transport and deposition is a common strategy to grow ZnO nanowire arrays, where the metal catalysts act as nucleation sites.[14] But, it is proved that gold can diffuse into the nanowire with its growth.[15,16] So, its effects on electrical and optical properties of nanowires and nanowire heterostructures should be carefully addressed.

In comparison with nanowires, there is no common growth strategy that can be applied for nanobelts and, therefore, growth of ZnO nanobelts is more difficult. It usually needs high temperature (1400–1450 °C) and long growth time (2–3 h).[17,18] In order to reduce the energy consumption with lower growth temperature, some groups used tin[19,20] or indium[3] as catalyst or dopant to synthesize ZnO nanobelts. There are also some groups using pure zinc chloride,[21] zinc sulfide,[22,23] or zinc-copper alloy[24] as source materials to grow ZnO nanobelts. Such growth methods are usually of much lower yield than nanowires and also inevitably introduce impurities into the nanobelts. So, in general, the obtained ZnO nanobelts are of lower optical quality.[20–23] Lu *et al.*[25] and Yang *et al.*[26] reported the hydrothermal and electrochemical growth methods for ZnO nanobelts with temperature as low as 150 °C. But, these obtained products by solution methods were usually mixture of nanowires and nanobelts and their optical properties were not studied.

Overall, although growth of ZnO nanowires/nanobelts is widely reported, the applied experimental conditions were rather diverse among different groups and morphologically controlled growth is still challenging and desired.[27] In this study, a simple but effective catalyst-tailored CVD method was demonstrated to grow ZnO nanowires and nanobelts in a controlled way. Moreover, the ZnO nanobelts grown without using any catalyst or dopant show different optical properties than nanowires grown with a gold-catalyst assisted VSL process.

2. Experimental

The ZnO nanostructures were synthesized with a chemical vapour deposition growth system. It comprises a standard quartz tube furnace with an inner diameter of 50 mm (Kyouei, Japan), a vacuum gauge (MSK, USA), two mass flow controllers (Ar and O_2, KOFLOC, Japan), and a pump station together with a needle valve. The source material was a mixture of ZnO and C powder (1 : 1 wt%) in ceramic boat and located in the middle of the quartz tube. Argon was used as carrier gas with flow rate of 100 standard cubic centimetre per minute (SCCM) and the pressure was maintained at 100 Torr. The heating up rate of the CVD furnace is 15 °C min^{-1} and the growth temperature was optimized in a range from 950–1000 °C. When temperature was below 950 °C, no products were obtained whilst temperatures higher than 1000 °C were not needed. The growth time at the

[a]*School of Materials Science and Engineering, University of Jinan, Jinan 250022, Shandong, China. E-mail: mse_caobq@ujn.edu.cn*
[b]*Graduate School of Information Science and Electrical Engineering, Kyushu University, Fukuoka 819-0395, Japan*
[c]*Cooperative Research Center, University of Miyazaki, Miyazaki 889-2192, Japan*

peak temperature was 25 min and then the furnace was cooled down naturally to room temperature. The pure silicon (100) substrates were first immersed into acetone and ethanol for two minutes, respectively, and then rinsed with distilled water and dried with nitrogen before put into the quartz tube. Some washed silicon wafers were used as substrates to deposit thin gold film of 2 nm with a thermal evaporation chamber (ULTRAVAC, Japan) and then were ready for ZnO sample growth.

The morphology and the crystalline structure of the as-fabricated ZnO nanostructures were characterized with a scanning electron microscope (SEM, VE-7800, Keyence) and a high-resolution transmission electron microscope with point resolution of 0.12 nm (HRTEM, 1300NEF, JEM). X-Ray powder diffraction (XRD) patterns were recorded on a Rigaku Multi-Flex diffractometer using Cu-Kα radiation. The PL spectra of the as-prepared ZnO structures were first measured at room temperature excited with the third harmonic of a Q-switched Nd:YAG laser (355 nm, 5 ns, 5 Hz, New Wave). The excitation power density was varied from 13 kW cm^{-2} up to 50 MW cm^{-2} by tuning the laser energy. The spectra were recorded by a spectrometer with 1200 lines per mm grating (Lambda Vision, Japan). For temperature-dependent PL measurements, a He–Cd laser (325 nm, 30 mW, Kimmon) was used as the excitation light source and the sample was placed in a cryostat for temperature control (10–200 K).

3. Results and discussion

3.1 Structural characterizations

Fig. 1(a) and Fig. 2(a) show the typical survey SEM images of the obtained samples. Together with the high-resolution SEM images shown in the insets, their different morphologies can be clearly identified. When gold was used as catalysts, quasi-aligned ZnO nanowire arrays were grown on silicon substrate. The diameters of these nanowires range from 80–120 nm and their lengths are of tens of micrometres. It is clearly demonstrated in Fig. 1(a) that nanowires can only selectively grow on the patterned gold thin film, which strongly suggests the nanowire growth is a gold-catalyst assisted VLS mechanism. However, when silicon substrates without any catalyst were used, random aligned nanobelts were grown instead of nanowires, as shown in Fig. 2(a). The belts are found to be several micrometres in length and about one micrometre in width with a thickness of tens of nanometres, as evidenced by a side-view SEM image shown in the inset of Fig. 2(a).

All the XRD peaks shown in Fig. 3 can be attributed to the hexagonal wurtzite ZnO, which confirms the pure phase of the obtained ZnO samples. An additional peak at 33° of Si(200) was detected from the substrate as shown in Fig. 3(b) due to the multiple X-ray scattering effect.[28] Clearly, the quasi-aligned ZnO nanowires show *c*-axis orientation. But, the $(10\bar{1}0)$-peak diffraction intensity of ZnO nanobelts is stronger than that of the standard ZnO powder X-ray diffraction pattern (JCPDS 36-1451). It means that the top and bottom surfaces of the nanobelts are $\{10\bar{1}0\}$-planes, which is consistent with the following TEM studies.

A further structural study of the as-prepared ZnO nanowires and nanobelts was conducted with an ultra-high voltage omega-filter TEM with lattice resolution of 0.12 nm. The general low-magnification TEM images shown in Fig. 1(b) and Fig. 2(b) confirm that the samples have wire and belt-like morphologies, respectively. For nanowires, the typical characters like single crystal and preferential growth along *c*-axis demonstrated by selected-area electron diffraction (SAED) and HRTEM images are similar to the former reports. But, the single-crystal nanobelt has a growth direction along *a*-axis enclosed by {0001} and $\{01\bar{1}0\}$ base planes, as indicated in Fig. 2(b), which is different to the typical *c*-axis growth direction of ZnO nanowires. Pan *et al.*[17] found that ZnO nanobelts have two different growth directions. One is along [0001] without defects and dislocations and another is $[01\bar{1}0]$ with a single stacking fault parallel to the nanobelt. But,

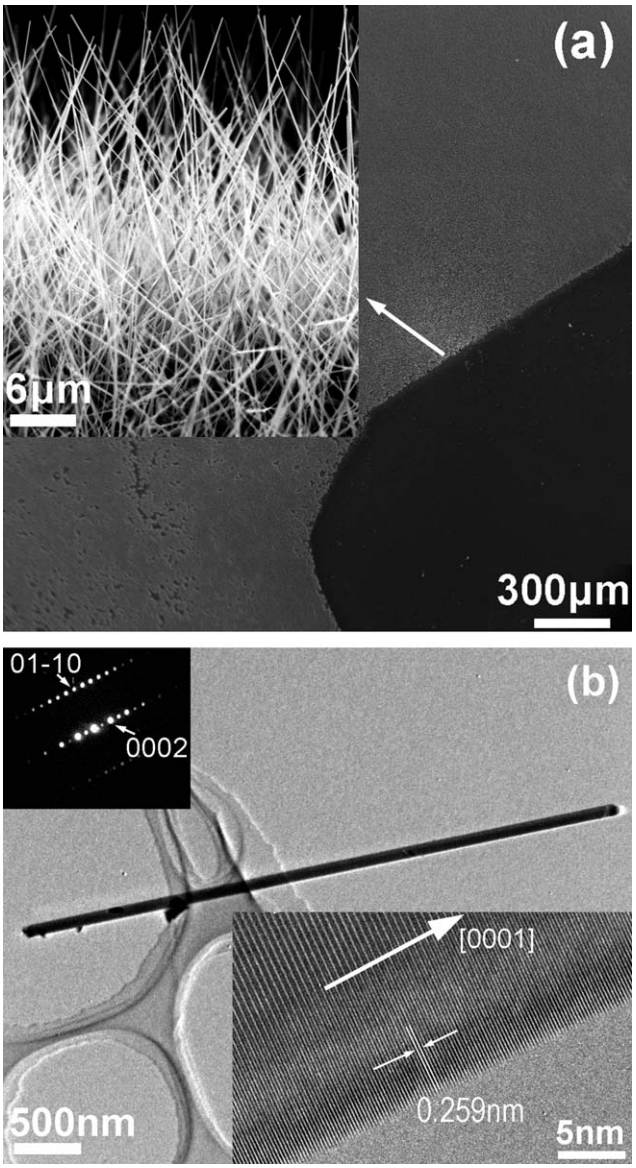

Fig. 1 (a) SEM image of the ZnO nanowires grown on silicon substrates. Selective growth is clearly shown using patterned gold as catalysts. Inset is a high-magnification SEM image of the ZnO nanowires. (b) TEM image of a ZnO nanowire. Left inset is the SAED pattern confirming the single-crystal of nanowire. Right inset is the HRTEM image showing clear lattice fringe of *c*-plane.

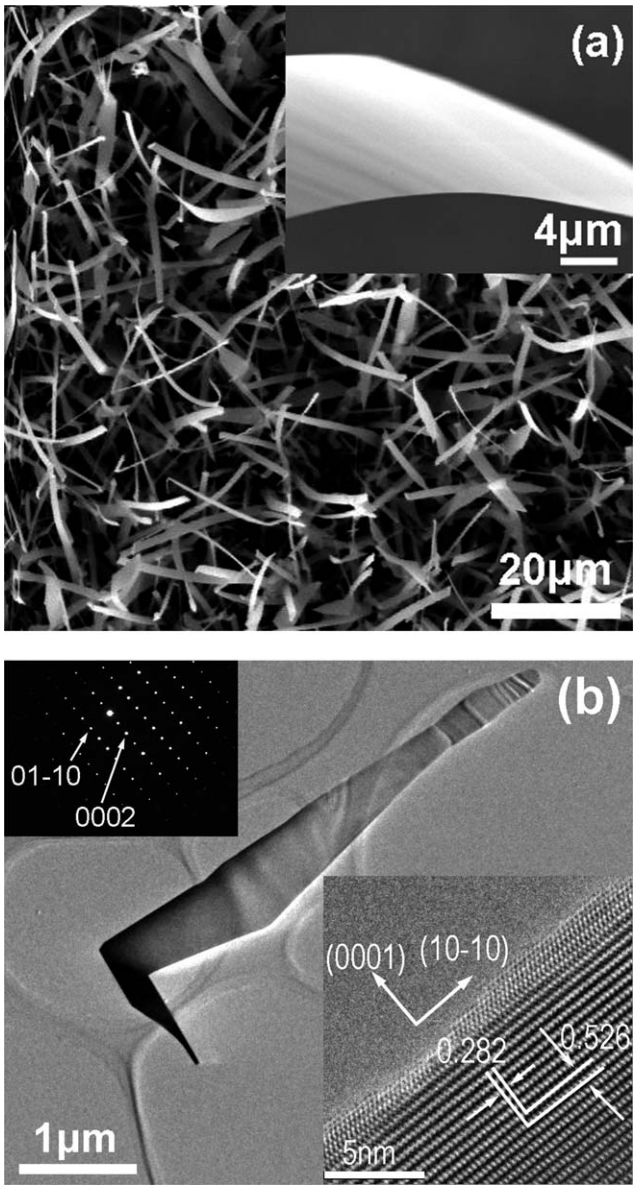

Fig. 2 (a) SEM image of the ZnO nanobelts grown on silicon substrates and inset is a high-magnification SEM image of a single nanobelt. (b) TEM image of a ZnO nanobelt displaying its shape characteristics. Right inset is the HRTEM image showing clear lattice fringe. Using the Digital Microscopy software, the lattice fringe distances were measured and marked. Left inset is the corresponding SAED pattern confirming the single-crystal of nanobelt. The basal planes of the nanobelts are $\{10\bar{1}0\}$ planes.

careful HRTEM observations on several nanobelts did not find visible defect or stacking fault in our samples. Moreover, the surface of the nanobelt is atomically sharp and without any sheathed amorphous phase, which both indicates the nanobelts are of good single crystal quality.

3.2 Growth mechanism

Depending on the metal catalyst used or not in the synthesis process, two growth mechanisms, *e.g.* VLS and VS, have been proposed for the growth of 1D nanostructures. The ZnO

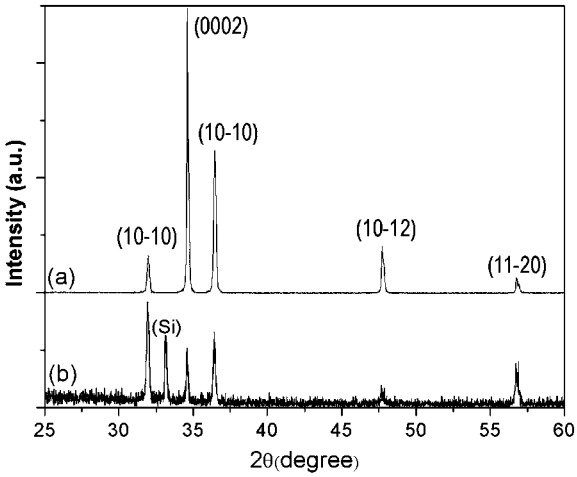

Fig. 3 (a) XRD spectrum of ZnO nanowire arrays showing partially *c*-axis preferential growth. (b) XRD spectrum of ZnO nanobelts on a silicon substrate with a diffraction peak from the substrate.

nanowire growth here can be attributed to the VLS mechanism, as the nanowire only grew selectively on the patterned gold catalyst. It was reported that ZnO nanobelts could also be grown with gold catalyst *via* VSL mechanism.[3,29] However, the source materials for nanobelt growth were intentionally doped with indium oxide. In our experiment, the VLS mechanism for nanobelt growth can be excluded as no extrinsic catalyst or dopant was used. Therefore, the formation of ZnO nanobelts should be attributed to the VS growth mechanism through homogenous nucleation.[30]

According to the homogenous nucleation theory, the two-dimensional (2D) nucleation rate was closely related to supersaturation ratio determined by the actual vapour pressure and the equilibrium vapour pressure.[31] When no catalyst was applied, the actual local pressure on silicon substrate was higher in comparison with the case of nanowire VLS-growth as the gold catalyst first absorbed the incoming vapour and then solid nanowire precipitated. So, the bigger supersaturation ratio caused by high pressure could result in higher 2D nucleation rate.[17] Once the 2D nuclei were formed, the newly arriving molecules continued to deposit on the formed nuclei and diffused easily due to their high mobility at temperature about 1000 °C. Finally, 2D nanobelts formed with low-energy surfaces, *e.g.* $\{01\bar{1}0\}$ planes, tended to be flat.

3.3 Different optical properties

Fig. 4 shows the normalized room-temperature PL spectra of ZnO nanowires and nanobelts under same measurement conditions. The UV emission at about 385 nm is the near-bandgap-edge (NBE) emission, which usually originates from the free exciton emission and its replicas.[32] The usually observed defect-related visible emission of ZnO was not detected, which means both the nanowires and nanobelts are of good optical quality.[33,34] However, the full width at half maximum (FWHM) of nanobelt is much smaller than that of nanowire, as shown in the inset of Fig. 4. The broadening of the NBE peak of nanowires implies that the UV emission cannot be simply attributed to the

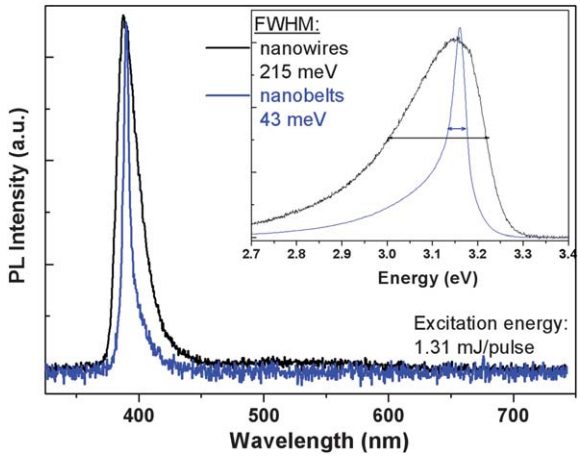

Fig. 4 Comparison of normalized room-temperature PL spectra of ZnO nanowires and nanobelts on a silicon substrate under same PL experimental conditions. Inset shows the FWHM of the nanobelt is smaller.

recombination of free excitons. To find the origin of this peak, series of temperature-dependent PL spectra were measured.

Fig. 5 shows the PL spectra measured at temperature from 10–200 K. The PL spectrum at $T = 10$ K of ZnO nanobelts shown in Fig. 5(a) are dominated by the emission peak at 3.359 eV that is a typical donor-bound excitons (D^0X).[35] On the high energy side of this peak, three small shoulders are observed which can be assigned to the free-exciton re-combinations as indexed with $FX^n_{A,B}$ ($n = 1, 2$). Two groups of phonon replica assigned as D^0X-nLO and FX-nLO ($n = 1, 2, 3, 4$) are observed with energy separation of 72 meV (LO-phonon energy) below the D^0X and FX peaks, respectively. The peak at 3.332 eV is due to the two-electron satellite (TES) transition.[36] With the increasing temperature, it is found that the intensities of the two series of peaks associated with FX and D^0X exhibit an opposite dependence on temperature. The intensities of FX and its related phonon replicas increase while the intensities of D^0X and its replicas decrease and are not detectable at temperature over 70 K. The fast intensity reduction of D^0X is a result of the rapid thermal ionization of bound excitons with increasing temperature. Therefore, more free excitons occupy the ground states and at room temperature the NBE peak is due to the recombination of free excitons.

Besides the general emission characters, the PL spectra of ZnO nanowires shown in Fig. 5(b) exhibit at least three different features to that of nanobelts. First, the peak of bound-exciton-complex (BEC) is rather wider than that of nanobelts. This difference could be due to an inhomogeneous broadening caused by spatially averaging the measured samples with different morphologies (*e.g.* different diameters) or crystalline qualities. In comparison with nanobelt samples, the diameters/shapes of the measured ZnO nanowires are more uniform. Therefore, the linewidth broadening is mainly caused by crystal quality. It means more donor/acceptor defects involved in the BEC. Second, the free exciton emission was not observed from the ZnO nanowires because of the localization of excitons by impurities or defects.[37] Third, a peak at 3.310 eV was detected, whose origin was formerly controversial in the past decade. Recently, it was proved that this emission was due to a free-to-bound transition

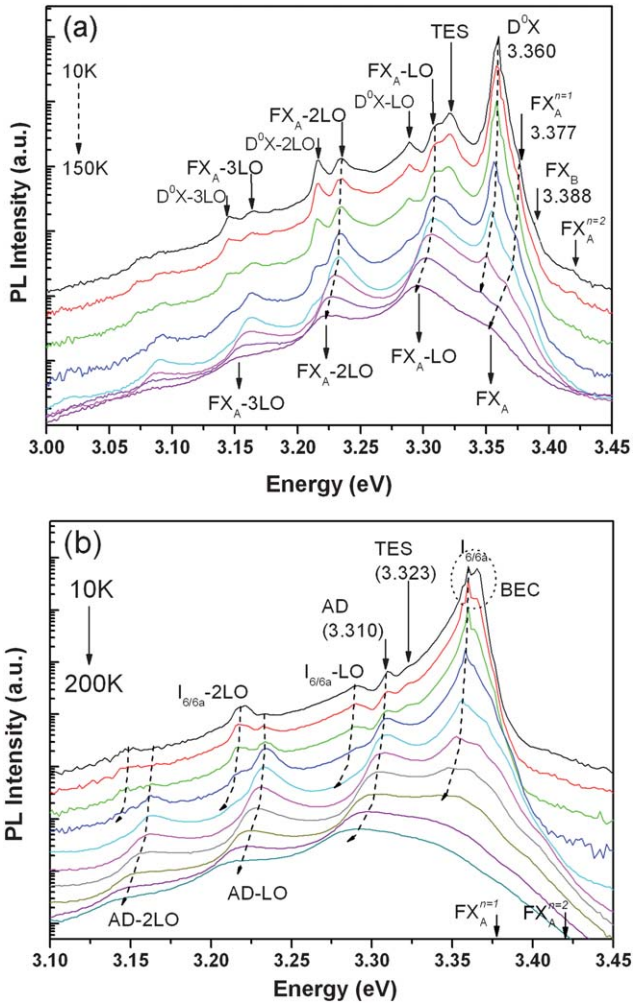

Fig. 5 Temperature-dependent PL spectra of ZnO nanobelts (a) and nanowires (b) measured from 10–200 K excited with a low-power (30 mW) He–Cd laser. The PL spectra were vertically shifted for clear vision. AD: acceptor-related defects. The energy spacing between two adjacent vertical dashed lines is 72 meV, the energy of longitudinal optical phonon of ZnO.

of electrons from conduction band to holes localizing at acceptor-related defects,[38] whose microstructure was still not clear. Considering the VLS growth mechanism, it introduces the high possibility to carry the metal catalysts into the nanowire.[39–41] Moreover, gold in particular is known to be deep traps/acceptors in semiconductors.[42] Here, we suggested that gold should be a very possible origin of these acceptor-related defects (AD) in the nanowires. Therefore, with temperature increasing, the transition from conduction band to deep acceptors dominated the NBG emission.

To further study the optical properties, the light amplification behaviours of ZnO nanowires and nanobelts were measured by varying the excitation density. Fig. 6(a) shows the PL spectra of ZnO nanobelts under excitation from 103 kW cm^{-2} to 6.97 MW cm^{-12}. The dependence of the peak intensity and FWHM on excitation density is shown in Fig. 6(b). At low excitation intensity smaller than 3 MW cm^{-2}, the PL spectra consist of a single broad and featureless spontaneous emission peak. The

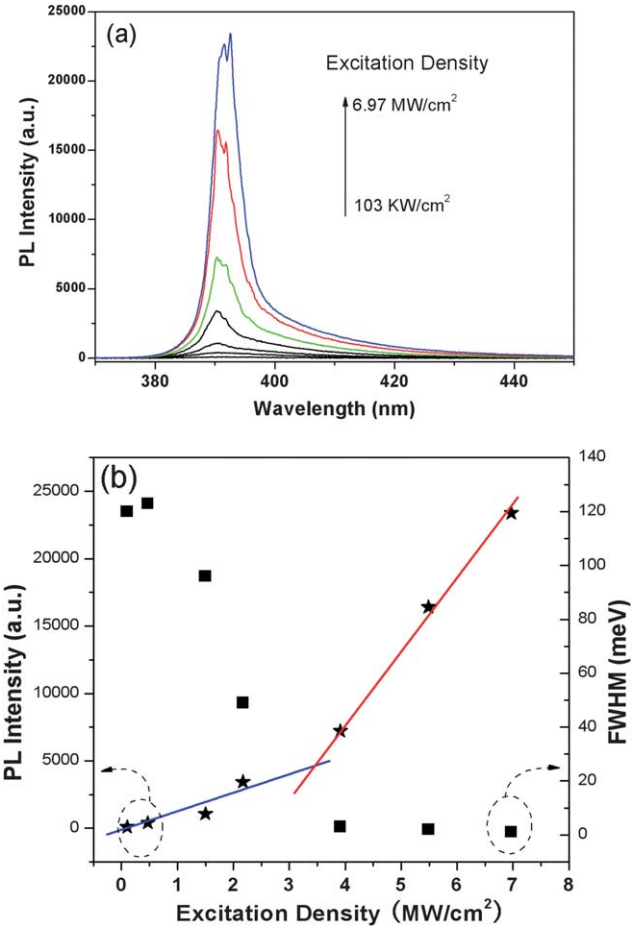

Fig. 6 (a) Room-temperature PL spectra evolution of ZnO nanobelts under different excitation densities from 0.103 to 6.97 MW cm^{-12}. (b) Dependence of peak intensity and FWHM on the excitation density. Lines are a guide for the eyes.

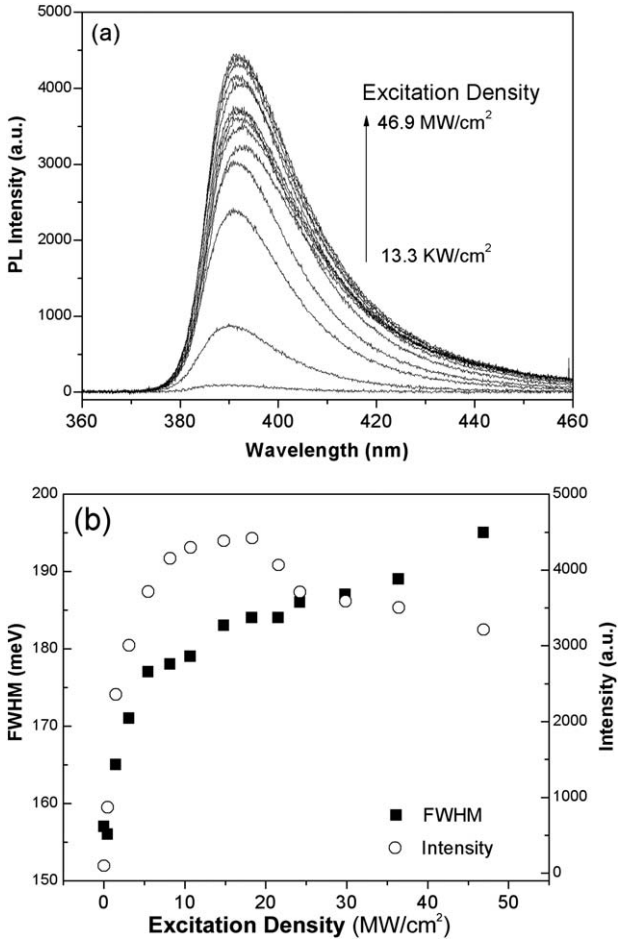

Fig. 7 (a) Room-temperature PL spectra of ZnO nanowires under different excitation densities from 0.013 to 46.9 MW cm^{-2} with a Nd:YAG laser (355 nm, 5 ns, 5 Hz). The typical SEM image of the measured ZnO nanowires was similar to Fig. 1. (b) Dependence of the peak intensity and FWHM on the excitation density.

emission peak became narrower when the excitation intensity was further increased. Very narrow peaks appeared and superimposed on the peak when the excitation intensity exceeded a threshold of about 4 MW cm^{-12}. The FWHMs of these sharp peaks were only about few nanometres. At the same time, the peak intensity shows super linear increase, which means laser actions. As for the lasing of ZnO nanobelts, two mechanisms can be expected, *e.g.* Fabry–Pérot (F–P) cavity and random lasing.[43,44] According to the F–P cavity theory, the relationship between the model spacing and the cavity length can be calculated with $\Delta\lambda_c = \lambda_1\lambda_2/2nL$, where n is the effective refractive index (2.3 for ZnO), L is the effective length of the cavity, and λ_1 and λ_2 are the two adjacent peaks. With the observations in Fig. 6(a) of $\lambda_1 = 391.8$ nm and $\lambda_2 = 390.5$ nm, the deduced cavity length is ~25 μm, which is consistent with the nanobelt length shown in Fig. 2(a). Therefore, the F–P cavity was expected to be formed between two crystalline planes along the nanobelt growth direction.

Fig. 7(a) shows the PL spectra of ZnO nanowires under excitation density from 13.3 kW cm^{-2} to 46.9 MW cm^{-12}. The dependence of the peak intensity and FWHM on the excitation density was shown in Fig. 7(b). The peak intensity of the nanowires first increased linearly, then saturated and finally decreased when the excitation density was increased. At the same time, the FWHM first increase fast then slowly. Clearly, no laser was observed from the ZnO nanowires. The first intensity increase can be easily understood as, with the excitation increasing, more electrons and holes (or excitons) were generated at the band edges with result of higher recombination probability. But, the later PL intensity saturation and decrease with excitation increasing is anomalous.

In general, the PL intensity saturation/decrease is due to non-radiative recombination, which is usually caused by the degradation of crystal quality and/or thermally activated non-radiative re-combinations. For polar ZnO, the electron-longitudinal optical (LO) phonon interaction (Fröhlich interaction) becomes stronger with the temperature increasing and LO phonons with higher order will contribute to the UV emission, as shown in the temperature-dependent PL of Fig. 5. The increase of PL FWHM of Fig. 7(b) indicates that the sample temperature increases under high excitation laser. It was proved that the temperature of ZnO nanostructure ensembles excited with a laser of ~1 MW cm^{-2} can be as high as 700 °C.[45] Therefore, with the sample temperature increasing induced by laser excitation, the trap/acceptor defect

centers in nanowires, as identified in Fig. 5(b), could act as thermally activated non-radiative emission centers with a result of the PL intensity saturation or decrease.

4. Conclusion

In summary, a simple but reliable catalyst-tailored CVD method was demonstrated to grow ZnO nanowires and nanobelts on silicon substrates and the nanobelts were proved to be of higher optical quality. ZnO nanowires grew along *c*-axis through the traditional catalyst-assisted VLS mechanism. But, ZnO nanobelts grew along *a*-axis without using any catalyst or dopant. The room-temperature NBG emission of nanobelts originated from the free exciton recombination and its replicas. While, the NBG emission of nanowires was due to the recombination of electrons from the conduction band to holes localizing at defects, which was due to the catalyst incorporation during the VLS growth process. Accordingly, laser emission was only observed from ZnO nanobelts. The anomalous PL intensity and FWHM dependence of nanowires on excitation density was consistent with the temperature-dependant PL results. Therefore, our results represent a rational growth method for different ZnO nanostructures and some advancement in the understanding of catalyst incorporation and doping in ZnO nanowires.

Acknowledgements

BC is a Taishan Scholar Endowed Professor and thanks the supports from NSFC (51002065), Shandong Distinguished Middle-aged and Young Scientist Encourage and Reward Foundation (BS2010CL003), and UJN for a new faculty. The work performed at Kyushu University are supported by a Grant-in-Aid for Scientific Research from the Japan Society for the Promotion of Science (JSPS, 20360142) and a Special Coordination Funds for Promoting Science and Technology from Japan Science and Technology Agency.

Reference

1 X. S. Fang, Y. Bando, U. K. Gautam, C. H. Ye and D. Golberg, *J. Mater. Chem.*, 2008, **18**, 509.
2 H. B. Zeng, X. J. Xu, Y. Bando, U. K. Gautam, T. Y. Zhai, X. S. Fang, B. D. Liu and D. Golderg, *Adv. Funct. Mater.*, 2009, **19**, 3165.
3 H. J. Fan, B. Fuhrmann, R. Scholz, C. Himcinschi, A. Berger, H. Leipner, A. Dadgar, A. Krost, S. Christiansen, U. Gösele and M. Zacharias, *Nanotechnology*, 2006, **17**, S231.
4 Y. B. Li, A. Paulsen, I. Yamada, Y. Koide and J. J. Delaunay, *Nanotechnology*, 2010, **21**, 295502.
5 S. Zhang, Y. Shen, H. Fang, S. Xu, J. H. Song and Z. L. Wang, *J. Mater. Chem.*, 2010, **20**, 10606.
6 B. Q. Cao, M. Lorenz, A. Rahm, H. von Wenckstern, C. Czekalla, J. Lenzner, G. Benndorf and M. Grundmann, *Nanotechnology*, 2007, **18**, 455707.
7 B. C. Cheng, Z. D. Zhang, H. J. Liu, Z. H. Han, Y. H. Xiao and S. J. Lei, *J. Mater. Chem.*, 2010, **20**, 7821–7826.
8 B. Q. Cao, J. Zúñiga–Pérez, C. Czekalla, H. Hilmer, J. Lenzner, N. Boukos, A. Travlos, M. Lorenz and M. Grundmann, *J. Mater. Chem.*, 2010, **20**, 3848.
9 A. Umar and Y. B. Hahn, *Nanotechnology*, 2006, **17**, 2174.
10 H. Q. Wang, G. H. Li, L. C. Jia, G. Z. Wang and C. J. Tang, *J. Phys. Chem. C*, 2008, **112**, 11738.
11 H. Q. Wang, G. Z. Wang, L. C. Jia, C. J. Tang and G. H. Li, *J. Phys. D: Appl. Phys.*, 2007, **40**, 6549.
12 Z. L. Wang, *Mater. Sci. Eng., R*, 2009, **64**, 33(Review).
13 C. Klingshirn, *Phys. Status Solidi B*, 2007, **244**, 3027(Review).
14 H. J. Fan, W. Lee, R. Scholz, A. Dadgar, A. Krost, K. Nielsch and M. Zacharias, *Nanotechnology*, 2005, **16**, 913.
15 R. X. Yan, D. Gargas and P. D. Yang, *Nature Phys.*, 2009, **3**, 569.
16 M. J. Tambe, S. Q. Ren and S. Gradečak, *Nano Lett.*, 2010, **10**, 4584.
17 Z. W. Pan, Z. R. Dai and Z. L. Wang, *Science*, 2001, **291**, 1947.
18 K. Bando, T. Sawabe, K. Asaka and Y. Masumoto, *J. Lumin.*, 2004, **108**, 385.
19 X. D. Wang, Y. Ding, C. J. Summers and Z. L. Wang, *J. Phys. Chem. B*, 2004, **108**, 8773.
20 R. Deng, X. T. Zhang, E. Zhang, Y. Liang, Z. Liu, H. Y. Xu and S. K. Hark, *J. Phys. Chem. C*, 2007, **111**, 13013.
21 J. Zhang, W. Y. Yu and L. D. Zhang, *Phys. Lett. A*, 2002, **299**, 276.
22 Z. G. Chen, F. Li, G. Liu, Y. B. Tang, H. T. Cong, G. Q. Lu and H. M. Cheng, *J. Nanosci. Nanotechnol.*, 2006, **6**, 704.
23 G. Z. Shen, D. Chen and C. J. Lee, *J. Phys. Chem. B*, 2006, **110**, 15689.
24 Y. B. Li, Y. Bando, T. Sato and K. Kurashima, *Appl. Phys. Lett.*, 2002, **81**, 144.
25 C. H. Lu, L. M. Qi, J. H. Yang, L. Tang, D. Y. Zhang and J. M. Ma, *Chem. Commun.*, 2006, 3551.
26 J. H. Yang, G. M. Liu, J. Lu, Y. F. Qiu and S. H. Yang, *Appl. Phys. Lett.*, 2007, **90**, 103109.
27 Z. L. Wang, *ACS Nano*, 2008, **2**, 1987.
28 J. Z. Tischler, J. D. Budai, G. E. Ice and A. Habenschuss, *Acta Crystallogr., Sect. A: Found. Crystallogr.*, 1988, **44**, 22.
29 J. S. Jie, G. Z. Wang, X. H. Han, Q. X. Yu, Y. Liao, G. P. Li and J. G. Hou, *Chem. Phys. Lett.*, 2004, **387**, 466.
30 Z. R. Dai, Z. W. Pan and Z. L. Wang, *Adv. Funct. Mater.*, 2003, **13**, 9.
31 H. J. Scheel and T. Fukuda, *Crystal Growth*; Wiley; West Sussex; 2003.
32 W. Shan, W. Walukiewicz, J. W. AgerIII, K. M. Yu, H. B. Yuan, H. P. Xin, G. Cantwell and J. J. Song, *Appl. Phys. Lett.*, 2005, **86**, 191911.
33 B. Q. Cao, W. P. Cai and H. B. Zeng, *Appl. Phys. Lett.*, 2006, **88**, 161101.
34 B. Q. Cao, W. P. Cai, H. B. Zeng and G. T. Duan, *J. Appl. Phys.*, 2006, **99**, 073516.
35 B. K. Meyer, H. Alves, D. M. Hofmann, W. Kriegseis, D. Forster, F. Bertram, J. Christen, A. Hoffmann, M. Straβburg, M. Dworzak, U. Haboeck and A. V. Rodina, *Phys. Status Solidi B*, 2004, **241**, 231.
36 K. Thonke, Th. Gruber, N. Teofilov, R. Sch. onfelder, A. Waag and R. Sauer, *Phys. B*, 2001, **308–310**, 945.
37 J. I. Pankove, *Optical Processes in Semiconductors* 1971, New York: Dover.
38 M. Schirra, R. Schneider, A. Reiser, G. M. Prinz, M. Feneberg, J. Biskupek, U. Kaiser, C. E. Krill, K. Thoke and R. Sauer, *Phys. Rev. B: Condens. Matter Mater. Phys.*, 2008, **77**.
39 R. J. H. Morris, M. G. Dowsett, S. H. Dalal, D. L. Baptista, K. B. K. Teo and W. I. Milne, *Surf. Interface Anal.*, 2007, **39**, 898.
40 M. C. Putnam, M. A. Filler, B. M. Kayes, M. D. Kelzenberg, Y. B. Guan, N. S. Lewis, J. M. Eiler and H. A. Atwater, *Nano Lett.*, 2008, **8**, 3109.
41 D. E. Perea, E. R. Hemesath, E. J. Schwalbach, J. L. Lensch-Falk, P. W. Voorhees and L. J. Lauhon, *Nat. Nanotechnol.*, 2009, **4**, 315.
42 H. G. Grimmeiss, *Annu. Rev. Mater. Sci.*, 1977, **7**, 341.
43 X. L. Xu, F. S. F. Brossard, D. A. Williams, D. P. Collins, M. J. Holmes, R. A. Taylor and X. T. Zhang, *Appl. Phys. Lett.*, 2009, **94**, 231103.
44 B. Q. Cao, K. Sakai, D. Nakamura, I. A. Palani, H. B. Gong, H. Y. Xu, M. Higashihata and T. Okada, *J. Phys. Chem. C*, 2011, **115**, 1702.
45 K. A. Alim, V. A. Fonoberov and A. A. Balandin, *Appl. Phys. Lett.*, 2005, **86**, 053103.